International Journal of Fatigue 31 (2009) 1858–1864

Contents lists available at ScienceDirect

International Journal of Fatigue

journal homepage: www.elsevier.com/locate/ijfatigue

Fatigue of 7075-T651 aluminum alloy under constant and variable amplitude loadings

E.U. Lee [a,*], G. Glinka [b], A.K. Vasudevan [c], N. Iyyer [d], N.D. Phan [a]

[a] Naval Air Warfare Center Aircraft Division, Patuxent River, MD 20670, USA
[b] University of Waterloo, Waterloo, Ontario, Canada N2L 3G1
[c] Office of Naval Research, Arlington, VA 22203, USA
[d] Technical Data Analysis, Inc., Falls Church, VA, USA

ARTICLE INFO

Article history:
Received 24 September 2008
Received in revised form 18 November 2008
Accepted 20 November 2008
Available online 7 December 2008

Keywords:
Fatigue crack growth
Constant and variable amplitude loadings
Stress ratio
Frequency
Load spectrum

ABSTRACT

The fatigue crack growth (FCG) behavior of 7075-T651 aluminum alloy was studied under constant and variable amplitude loadings in vacuum, air and 1% NaCl solution. In the study of constant amplitude loading fatigue, the stress ratios were 0.1 and 0.85 and the loading frequency was 10 Hz. In the study of variable amplitude loading fatigue, the load spectrums were tension type and tension–compression type, and the average loading frequency was about 5 Hz. The results of FCG tests, under constant and variable amplitude loadings, validated the unified two parameter driving force model, accounting for the residual stress and stress ratio effects on fatigue crack growth.

Published by Elsevier Ltd.

1. Introduction

Fatigue crack growth in metallic materials is controlled by intrinsic factors, such as material property and microstructure, and extrinsic factors, such as environment and loading condition.

For a given material, it is well established that corrosive environments can accelerate the FCG [1–6]. This is attributable to a combination of anodic dissolution and hydrogen embrittlement at the crack tip. The latter is believed to result from a sequential process [7]: access of active species to the crack tip, adsorption, surface dissociation and hydrogen production, hydrogen entry and transport at the crack tip, and embrittling reaction. On the other hand, a corrosive environment can also cause fatigue crack growth retardation or arrest [8–10]. Three mechanisms have been proposed to account for this effect, which can occur in several material–environment combinations. One of them is crack blunting, which reduces the stress intensity factor, K, and hence cause crack growth retardation [8,11]. The second one is crack branching, which also decrease the stress intensity factor [9,12]. The third one is corrosion product wedging, which increases the minimum stress intensity factor and hence reduces the stress intensity range [10,13]. The amount of corrosion product wedging depends on the supply of dissolved oxygen.

Many structural components experience variable amplitude load histories, containing periodic overload and/or underload cycles. For example, hard landings, severe turbulence or harsh maneuvers during flight would be seen as overloads in the loading history of an aircraft. The load history effects, such as crack growth retardation following a tensile overload and crack growth acceleration following a compressive underload, are known to stem from plastic deformation in the vicinity of the crack tip [14–16] and to be closely related to the elastic–plastic behavior of the material [16–18]. To account for the load spectrum sequence effects, cycle-by-cycle FCG predictive models were developed. Those models can be divided into three main groups. The first group is classed as the yield zone model type, which include the Willenborg [19] and Wheeler [20] models. Both models consider that the current cyclic crack tip plastic zone develops inside a larger zone created by the preceding overload. However, their concepts and algorithms are different. The second group is based on crack closure, and includes plasticity-induced crack closure models [21] and strip yield models [22]. The third group, the unified two parameter model or UniGrow model, is based on the elastic–plastic crack tip stress–strain history [23,24].

The UniGrow model regards the FCG as a process of successive crack re-initiation in the crack tip region, controlled by a two parameter driving force. The driving force is derivable on the basis of the local stress and strain at the crack tip, using the Coffin–Manson strain–life law [25,26], Ramberg–Osgood relation [27] and Smith–Watson–Topper fatigue damage parameter [28]. The basic equation of this model for fatigue crack growth is

* Corresponding author. Tel.: +1 301 342 8069; fax: +1 301 342 8062.
E-mail address: eun.lee@navy.mil (E.U. Lee).

0142-1123/$ - see front matter Published by Elsevier Ltd.
doi:10.1016/j.ijfatigue.2008.11.013

$$da/dN = C[(K_{max,tot})^p(\Delta K_{tot})^{(1-p)}]^\gamma = C[\Delta k]^\gamma \quad (1)$$

where

$$C = 2\rho^*[(\psi_{y,1})^2/2^{(n'+3)/(n'+1)}\sigma'_f\varepsilon'_f\pi E\rho^*]^{-\{1/(b+c)\}}$$
$$p = n'/(n'+1), \quad \gamma = -2/(b+c)$$

a: crack length, b: fatigue strength exponent, c: fatigue ductility exponent, C: fatigue crack growth constant, da/dN: crack growth rate, E: modulus of elasticity, $K_{max,tot}$: total maximum stress intensity factor, ΔK_{tot}: total stress intensity range, n': cyclic strain hardening exponent, p: driving force constant, ε'_f: fatigue ductility coefficient, γ: fatigue crack growth equation exponent, ρ^*: notch tip radius or elementary material block size, σ'_f: fatigue strength coefficient, ψ_i: the averaging constant corresponding to the ith elementary block.

This model can predict the FCG and the effect of mean stress, including the influence of the applied compressive stress, without introducing the crack closure concept.

In this study, special emphasis is given to the clarification of the effects of stress ratio, load history and environment on FCG. FCG tests are performed under constant and variable amplitude loadings in three environments to find the combined effect of load history and environment. In addition, the test results are compared with the FCG prediction by the UniGrow model [23,24] to examine how closely the model can account for the load history effect in different environments.

2. Experiments

2.1. Specimen

In this study, compact-tension C(T) and middle-tension M(T) specimens were used for the constant and variable amplitude loading fatigue tests, respectively.

The compact-tension C(T) specimen, 38 mm (1.5 in.) wide and 9.5 mm (3/8 in.) thick, was machined from a 7075-T651 aluminum alloy plate, 32 mm (1.25 in.) thick, in L–T orientation. Its mechanical properties were UTS 570–574 MPa (82.7–83.2 ksi), YS 496–506 MPa (72.0–73.4 ksi) and elongation 12.5–13.0%.

The middle-tension M(T) specimen was machined in L–T orientation from a 7075-T651 aluminum alloy extrusion of 127 mm × 127 mm × 394 mm (5 in. × 5 in. × 15.5 in.).

It was 102 mm (4 in.) wide, 235 mm (9.3 in.) long and 2 mm (0.086 in.) thick, and its center notch was 3 mm (1/8 in.) long. Its mechanical properties were UTS 538 MPa (78 ksi), YS 446 MPa (65 ksi) and elongation 11%.

2.2. Test procedures

For the fatigue tests, three closed-loop servo-hydraulic mechanical test machines were employed. One was a 45 KN (10 kip) horizontal mechanical test machine for the fatigue test of C(T) specimens in air and 1% NaCl solution. The other two were 490 KN (110 kip) vertical MTS machines. One of them, equipped with a vacuum system, was used for the fatigue tests of C(T) and M(T) specimens in vacuum, and the other for the fatigue tests of M(T) specimens in air and 1% NaCl solution. In the case of fatigue test in 1% NaCl solution, the NaCl solution was circulated between a container of a C(T) specimen or a cup attached to a M(T) specimen and a reservoir by a pump without aerating. Each test machine was suitably interfaced with a computer system for automatic monitoring of fatigue load and crack growth, employing either compliance for C(T) specimens or DC potential drop technique for M(T) specimens.

The constant amplitude loading fatigue test with a C(T) specimen was conducted under stress control in tension–tension cycling of stress ratios 0.1 and 0.85. The growing crack length was measured, employing compliance technique. The fatigue loading procedure was K-decreasing (or load shedding) with K-gradient parameter $C = -0.08\ mm^{-1}$ ($-2\ in.^{-1}$) in the near-threshold crack growth regime and K-increasing with $C = 0.08\ mm^{-1}$ ($2\ in.^{-1}$) in the other regime, respectively.

The variable amplitude loading fatigue test with a M(T) specimen was performed under two different spectrum loadings, tension type and tension–compression type, Fig. 1. The growing crack length was measured, employing DC potential drop technique. The main features of the load spectrums are:

- Tension Type
  - Maximum Stress = 200.9 MPa (29.1 ksi)
  - Minimum Stress = −73.7 MPa (107 ksi)
  - Number of Stress Cycles/Pass = 2,249,614 cycles
- Tension–Compression Type
  - Maximum Stress = 162.3 MPa (23.5 ksi)

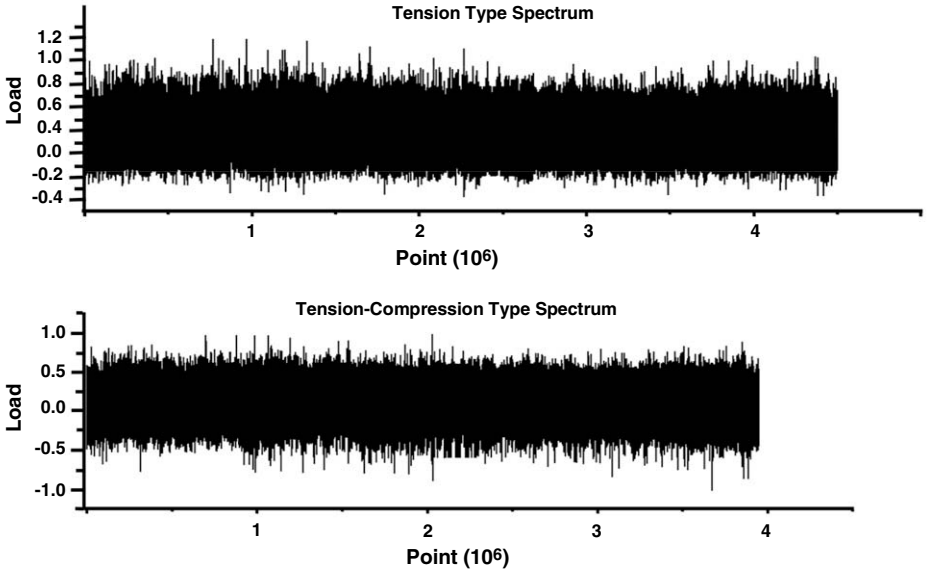

Fig. 1. Tension type and tension–compression type load spectrums.

Minimum Stress = −163.7 MPa (−23.7 ksi)
Number of Stress Cycles/Pass = 1,975,035 cycles

Three identical tests were done in each of the air and 1% NaCl solution environments under the two different spectrum loadings. However, because of the long test time, only one test was done under the tension type spectrum loading and two tests under the tension–compression type spectrum loading in vacuum. The averaged test results are presented in this paper.

The test environments for the constant and variable amplitude loading fatigue tests were vacuum of 4×10^{-8} torr, laboratory air of relative humidity about 50% and aqueous 1% NaCl solution of pH 2 at ambient temperature. The loading frequencies were 10 Hz for the constant amplitude loading fatigue test and about 5 Hz for the variable amplitude loading fatigue test.

3. Experimental results

3.1. Constant amplitude loading fatigue

The variation of fatigue crack growth rate da/dN with applied stress intensity range ΔK is shown in Fig. 2 for the fatigue tests at stress ratios $R = 0.1$ and 0.85 in vacuum, air and 1% NaCl solution. With R increasing from 0.1 to 0.85, the curve of da/dN vs. ΔK shifts to the left, increasing the da/dN and decreasing the threshold stress intensity range for fatigue crack growth ΔK_{th}, in the three environments. The environmental effect on the variation of da/dN with ΔK is shown in Fig. 3 for $R = 0.1$ and 0.85. At lower ΔK, the da/dN is greatest in 1% NaCl solution, slightly lower in air and much lower in vacuum. Correspondingly, the ΔK_{th} is least in 1% NaCl, slightly greater in air and greatest in vacuum. However, as the da/dN or the ΔK increases, the air and 1% NaCl solution curves shift towards the vacuum curve and the three curves tend to converge. At both $R = 0.1$ and 0.85, the air curve is closer to the 1% NaCl solution curve than to the vacuum curve, indicating air-assisted fatigue crack growth.

3.2. Variable amplitude loading fatigue

The variation of half crack length with number of loading cycle is shown in Fig. 4 for the fatigue tests under tension type and tension–compression type spectrum loadings in vacuum, air and 1% NaCl solution. Under the tension type spectrum loading, the crack growth is fast in air, slightly slower in 1% NaCl solution and much slower in vacuum. However, under the tension–compression type spectrum loading, the crack growth is fast in 1% NaCl solution, slightly slower in air and much slower in vacuum. From this observation, especially the similar high crack growth rates, the fatigue crack growth appears to be environmentally-assisted in air and 1% NaCl solution under the both spectrum loadings.

Fig. 5 compares the fatigue crack growths under the tension type and tension–compression type spectrum loadings in vacuum, air and 1% NaCl solution. The crack grows faster under the tension–compression type spectrum loading than under the tension type spectrum loading in the three environments.

3.3. Comparison of test result and prediction

The results of the tension type spectrum loading tests in vacuum and 1% NaCl solution are compared with the predictions by the UniGrow model [23,24] in Figs. 6 and 7, respectively. In vacuum, the test data and prediction are in good agreement in the first half life, there is some discrepancy between them growing with increasing number of loading cycle in the second half life, and the prediction life is longer than the test life, Fig. 6. In 1% NaCl solution, the test data and prediction are in good agreement in the

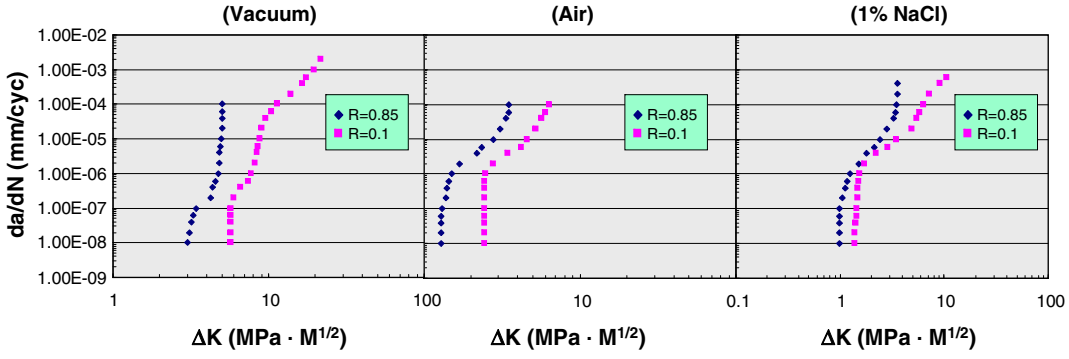

Fig. 2. da/dN vs. ΔK curves for constant amplitude loading, indicating stress ratio effect, in vacuum, air and 1% NaCl solution.

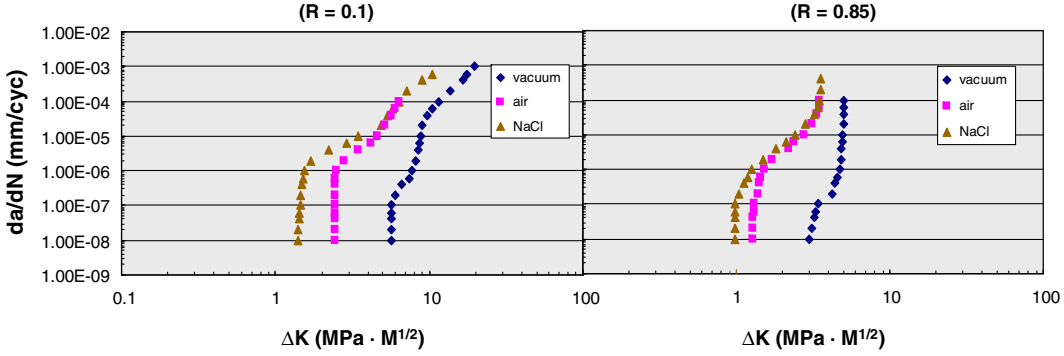

Fig. 3. Comparison of da/dN vs. ΔK curves for constant amplitude loading in vacuum, air and 1% NaCl solution.

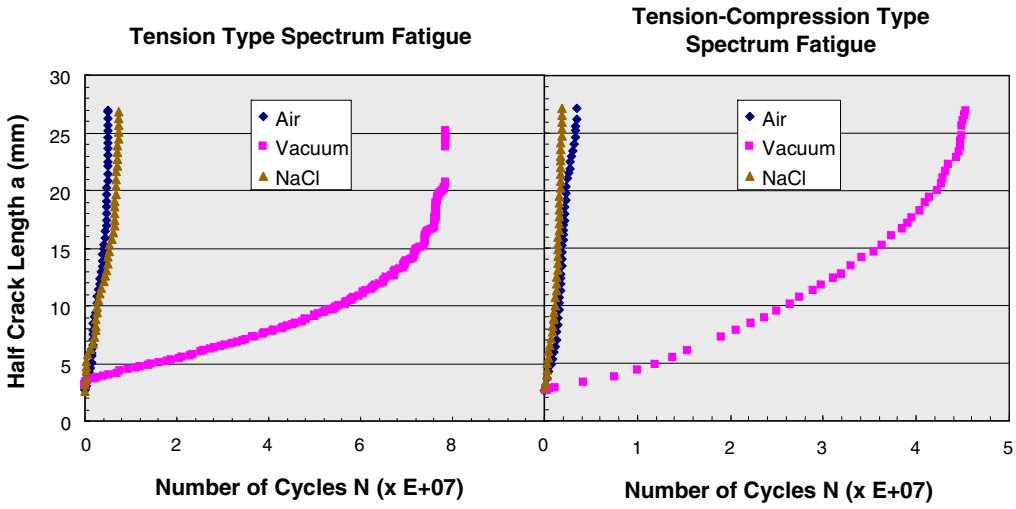

Fig. 4. Variation of half crack length *a* with loading cycle *N* for tension type and tension–compression type spectrum loadings in vacuum, air and 1% NaCl solution.

early stage of fatigue crack growth, but the predicted life is shorter than the test life, Fig. 7.

3.4. Fractography

Typical SEM fractographs of a specimen, which was subjected to the tension type spectrum loading in air are shown in Fig. 8. The fractographs show the areas of machined notch, pre-cracking and crack growth. Fatigue striations of variable spacing, are visible, faintly in the early stage of fatigue crack growth and clearly in the later stage. Another SEM fractograph of a specimen, which was tested under the same spectrum loading in 1% NaCl solution, shows fracture surface covered by corrosion product and faint striations, Fig. 9.

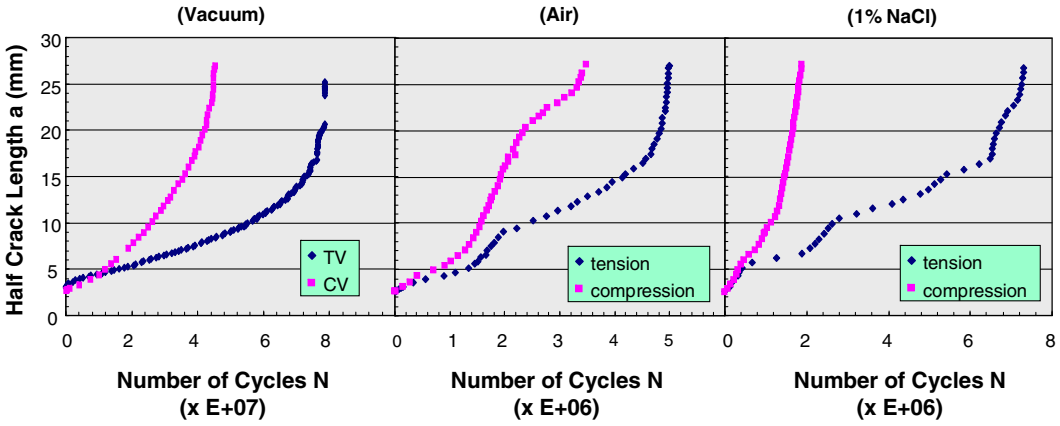

Fig. 5. Comparison of a vs. *N* curves for tension type and tension–compression type spectrum loadings in vacuum, air and 1% NaCl solution.

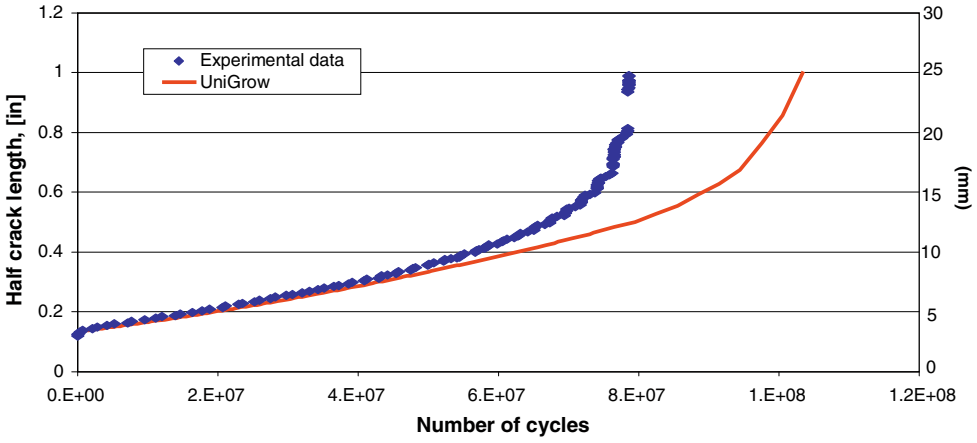

Fig. 6. Comparison of test data and UniGrow model prediction for the fatigue test under tension type spectrum loading in vacuum.

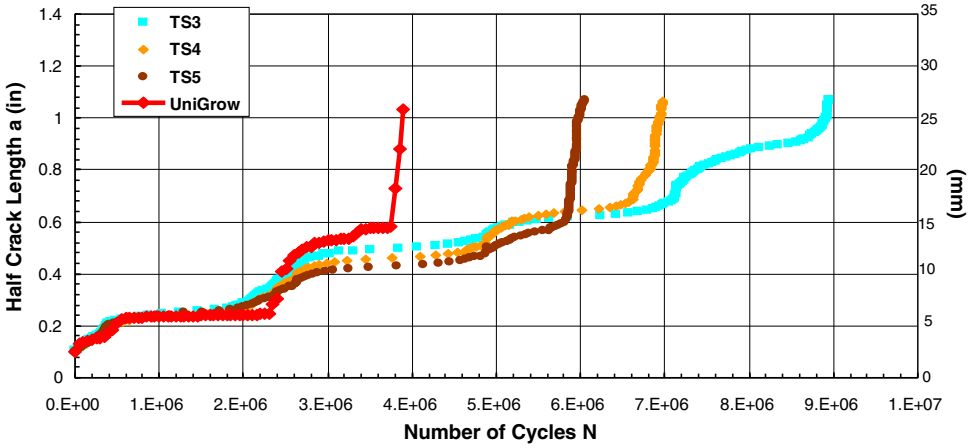

Fig. 7. Comparison of test data and UniGrow model prediction for the fatigue test under tension type spectrum loading in 1% NaCl solution.

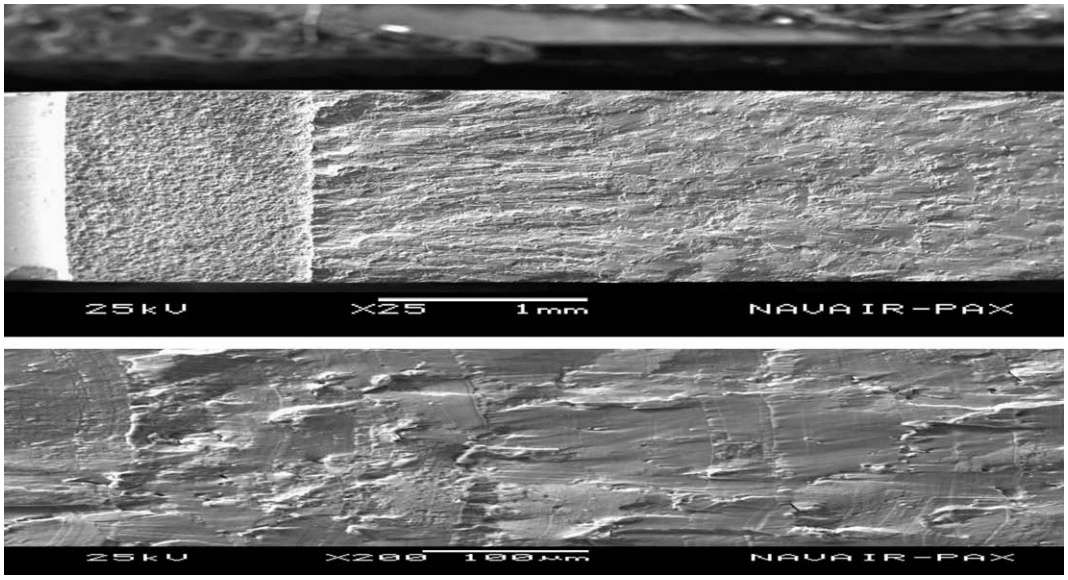

Fig. 8. SEM fractograph of a specimen, fatigue-tested under tension type spectrum loading in air.

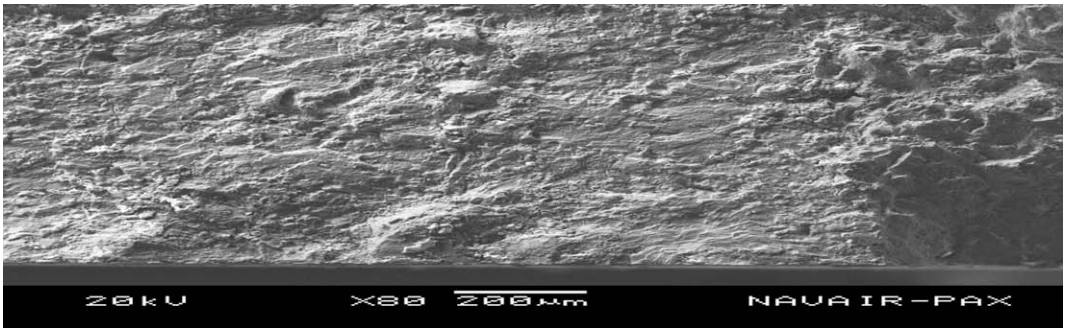

Fig. 9. SEM fractograph of a specimen, fatigue-tested under tension type spectrum loading in 1 % NaCl solution.

4. Discussion

4.1. Constant amplitude loading fatigue

The increase in stress ratio R from 0.1 to 0.85 was observed to increase the da/dN and decrease the ΔK_{th} in the three environments, as shown in Fig. 2. This observation is in agreement with the others' for various alloys [29–39].

Compared to vacuum, air and 1% NaCl solution induced similar corrosion fatigue behaviors, having close and lower ΔK_{th} values and accelerating FCG, in the near-threshold FCG regime, Fig. 3. This is attributable to their detrimental roles, anodic dissolution and

hydrogen embrittlement at the crack tip by NaCl solution, and adsorption of water vapor in air on crack tip surface and hydrogen embrittlement of cyclically deformed material within the plastic zone [29,39].

4.2. Variable amplitude loading fatigue

Similar to the one under constant amplitude loading, the FCG under variable amplitude loading is close and faster in air and 1% NaCl solution than in vacuum, Fig. 4. This evidences that the environmentally-assisted FCG also occurs under the variable amplitude loading. However, the FCG is slightly slower in 1% NaCl solution than in air under the tension type spectrum loading, whereas the reverse is observable under the tension–compression type spectrum loading, Fig. 4. The slower fatigue crack growth in 1% NaCl solution than in air is attributed to the corrosion-product-induced crack closure [40,41] under the tension type spectrum loading. It has been understood that the environmentally-assisted FCG is controlled by two concurrent and mutually competitive processes: corrosion-product-induced crack closure and embrittlement, occurring concomitantly with the crack tip oxidation in the corrosive medium [41]. Apparently, the corrosion-product-induced crack closure is more dominant than the embrittlement under the tension type spectrum loading, whereas the reverse is true under the tension–compression type spectrum loading and constant amplitude loading.

From the observed faster FCG under the tension–compression type spectrum loading than under the tension type spectrum loading, Fig. 5, it is clear that the FCG was retarded under the tension type spectrum loading and it was accelerated under the tension–compression type spectrum loading. The tension type load spectrum contains overload cycles of highest stress 200.9 MPa and the tension–compression type load spectrum contains underload cycles of minimum stress −163.7 MPa. These overloads and underloads are believed to be associated primarily with the observed retardation and acceleration of FCG under the tension type and tension–compression type spectrum loadings, respectively, in vacuum, air and 1% NaCl solution. A number of investigators also have reported the FCG retardation by tensile overload and acceleration by compressive underload [16,42–46].

In the comparison of the test result and the UniGrow model prediction, some discrepancies were found, as shown in Figs. 6 and 7. One of them, the shorter spectrum fatigue test life in vacuum than the prediction, Fig. 6, is attributable to the lack of constant amplitude loading fatigue test data at high ΔK, Fig. 2. The other, the longer spectrum fatigue test life in 1% NaCl solution than the prediction, Fig. 7, is attributable to the assumption of the same environmental effect under the both constant and variable amplitude loading conditions.

5. Summary and conclusion

- The da/dN increases and the ΔK_{th} decreases with increasing R under constant amplitude loading in vacuum, air and 1% NaCl solution.
- At lower ΔK, the da/dN is high in 1% NaCl solution, slightly lower in air, and much lower in vacuum under constant amplitude loading, indicating the FCG assisted by air and 1% NaCl solution.
- The FCG is close and fast in air and 1% NaCl solution and quite slow in vacuum under the tension type and tension–compression type spectrum loadings, evidencing the FCG assisted by air and 1% NaCl solution.
- The FCG is slower in 1% NaCl solution than in air, evidencing a crack growth retardation due to corrosion-product-induced crack closure in 1% NaCl solution, under the tension type spectrum loading. On the other hand, the reverse is observable under the tension–compression type spectrum loading.
- The tension type spectrum loading, containing tensile overloads, retards the FCG, whereas the tension–compression type spectrum loading, containing underloads, accelerates it, in vacuum, air and 1% NaCl solution.
- There are some discrepancies between the test result and UniGrow model prediction. These discrepancies are attributable to the lack of constant amplitude loading fatigue data at high ΔK in vacuum and the assumption of the same environmental effect under constant and variable amplitude loading conditions in 1% NaCl solution.

References

[1] Shen H, Podlaseck SE, Kramer IR. Effect of vacuum on the fatigue life of aluminum. Acta Metall 1966;14(March):341–6.
[2] Duquette DJ, Gell M. The effect of environment on the mechanism of stage I: fatigue fracture. Metall Trans 1971;2(May):1325–31.
[3] Mendez J, Demulsant X. Influence of environment on low cycle fatigue damage in Ti–6Al–4V and Ti 6246 titanium alloys. Mater Sci Eng A 1996;219(1–2):202–11.
[4] Mendez J. On the effects of temperature and environment on fatigue damage processes in Ti alloys and in stainless steel. Mater Sci Eng A 1999;263(2):187–92.
[5] Jaske CE, Broek D, Slater JE, Anderson WE. Corrosion fatigue of structural steels in seawater and for offshore applications. In: Corrosion fatigue technology, ASTM STP 642. American Society for Testing and Materials; 1978. p. 19–47.
[6] Henaff G, Odemer G, Tonneau-Morel A. Environmentally-assisted fatigue crack growth mechanisms in advanced materials for aerospace applications. Int J Fatigue 2007;29:1927–40.
[7] Wei RP, Simmons GW. Recent progress in understanding environment-assisted fatigue crack growth. Int J Fract 1981;17(2):235–47.
[8] Radon JC, Branco CM, Culver LE. Crack blunting and arrest in corrosion fatigue of mild steel. Int J Fract 1976;12:467–9.
[9] Tu LKL, Seth BB. Threshold corrosion fatigue crack growth in steels. J Test Eval 1978;6(1):66–74.
[10] Nordmark GE, Fricke WG. Fatigue crack arrest at low stress intensities in a corrosive environment. J Test Eval 1978;6(5):301–3.
[11] Creager M, Paris PC. Elastic field equations for blunt cracks with reference to stress corrosion cracking. Int J Fract Mech 1967;3:247–52.
[12] Vitek V. Plane strain intensity factors for branched cracks. Int J Fract 1977;13:481–501.
[13] Vasudevan AK, Suresh S. Influence of corrosion deposits on near-threshold fatigue crack growth behavior in 2xxx and 7xxx series aluminum alloys. Metall Trans A 1982;13A:2271–80.
[14] Elber W. The significance of fatigue crack closure. In: Damage tolerance in aircraft structures ASTM STP 486. American Society for Testing and Materials; 1971. p. 230–42.
[15] Wheeler O. Spectrum loading and crack growth. J Basic Eng 1972;94:181–6.
[16] Skorupa M. Load interaction effects during fatigue crack growth under variable amplitude loading – a literature review Part II: qualitative interpretation. Fatigue Fract Eng Mater Struct 1999;22(10):905–26.
[17] Pommier S. Cyclic plasticity and variable amplitude fatigue. Int J Fatigue 2003;25(9–11):983–97.
[18] Pommier S, DeFreitas M. Effect on fatigue crack growth of interactions between overloads. Fatigue Fract Eng Mater Struct 2002;25:709.
[19] Willenborg J, Engle RM, Wood HA. A crack growth retardation model using an effective stress concept. AFFDL-TR71-1. Air Force Flight Dynamic Laboratory, Wright-Patterson Air Force Base; 1971.
[20] Wheeler OE. Spectrum loading and crack growth. J Basic Eng 1972;94:181–6.
[21] Elber W. Fatigue crack closure under cyclic tension. Eng Fract Mech 1970;2:37–45.
[22] Dougdale DS. Yielding of steel sheets containing slits. J Mech Phys Solids 1960;8:100–8.
[23] Vasudevan AK, Sadananda K, Glinka G. Critical parameters for fatigue damage. Int J Fatigue 2001;23:S39–53.
[24] Noroozi AH, Glinka G, Lambert SA. A two parameter driving force for fatigue crack growth analysis. Int J Fatigue 2005;27:1277–96.
[25] Coffin LF. A study of the effects of cyclic thermal stresses on a ductile metal. Trans ASME 1954;76:931–50.
[26] Manson SS. Behavior of materials under conditions of thermal stress. NACA Report 1170, 1954.
[27] Ramberg W, Osgood WR. Description of stress–strain curves by three parameters. NACA, Technical Note No. 902, July 1943.
[28] Smith KN, Watson P, Topper TH. A stress–strain function for the fatigue of metals. J Mater, JMLSA 1970;5(4):767–78.
[29] Kirby BR, Beever CJ. Slow fatigue crack growth and threshold behaviour in air and vacuum of commercial aluminum alloys. Fatigue Eng Mater Struct 1979;1:203–15.

[30] Vasudevan AK, Bretz PE. Near-threshold fatigue crack growth behavior in 7XXX and 2XXX alloys: a brief review. In: Davidson DL, Suresh S, editors. Fatigue crack growth threshold concepts. Warrendale, PA: The Metallurgical Society of AIME; 1984. p. 25–42.
[31] Ritchie RO, Suresh S, Moss CM. Near-threshold fatigue crack growth in 2 ¼ Cr-1Mo pressure vessel steel in air and hydrogen. J Eng Mater Technol, ASME Trans 1980;102:293–9.
[32] Stewart AT. The influence of environment and stress ratio on fatigue crack growth at near threshold stress intensities in low-alloy steels. Eng Fract Mech 1980;13:463–78.
[33] Nakai Y, Tanaka K, Nakanishi T. The effects of stress ratio and grain size on near-threshold fatigue crack propagation in low-carbon steel. Eng Fract Mech 1981;15(3–4):291–302.
[34] Liaw PK, Saxena A, Swaminathan VP, Shih TT. Influence of temperature and load ratio on near-threshold fatigue crack growth behavior. In: Davidson DL, Suresh S, editors. Fatigue crack growth threshold concepts. Warrendale (PA): The Metallurgical Society of AIME; 1984. p. 205–23.
[35] Liaw PK, Leax TR, Donald JK. Fatigue crack growth behavior of 4340 steels. Acta Metall 1987;35(7):1415–32.
[36] Cadman AJ, Nicholson CE, Brook R. Influence of R ratio and orientation on the fatigue crack threshold (ΔK_{th} and subsequent crack growth of a low-alloy steel. In: Davidson DL, Suresh S, editors. Fatigue crack growth threshold concepts. Warrendale (PA): The Metallurgical Society of AIME; 1984. p. 281–98.
[37] Ritchie RO. Near-threshold fatigue crack propagation in ultra-high strength steel: influence of load ratio and cyclic strength. J Eng Mater Technol, ASME Trans; 1977:195–204.
[38] Suresh S, Vasudevan AK, Bretz PE. Mechanisms of slow fatigue crack growth in high strength aluminum alloys: role of microstructure and environment. Metall Trans A 1984;15A:369–79.
[39] Lee EU, Vasudevan AK, Sadananda K. Effects of various environments on fatigue crack growth in Laser formed and IM Ti–6Al–4V alloys. Int J Fatigue 2005;27:1597–607.
[40] Van der Velden R, Ewalds HL, Schultze WA. Anomalous fatigue crack growth retardation in steels for offshore applications. In: Crooker TW, Leis BN, editors. Corrosion fatigue, mechanics, metallurgy, electrochemistry, and engineering. ASTM STP 801. American Society for Testing and Materials; 1983. p. 64–80.
[41] Vasudevan AK, Suresh S. Influence of corrosion deposits on near-threshold fatigue crack growth behavior in 2XXX and 7XXX series aluminum alloys. Metall Trans A 1982;13A:2271–80.
[42] Skorupa M. Load interaction effects during fatigue crack growth under variable amplitude loading – a literature review, part I: empirical trends. Fatigue Fract Eng Mater Struct 1998;21:987–1006.
[43] Sadananda K, Vasudevan AK, Holtz RL, Lee EU. Analysis of overload effects and related phenomena. Int J Fatigue 1999;21:S233–46.
[44] Willenborg S, Eagle RM, Wood HA. A crack growth retardation model using an effective stress concept. AFFDL-TM-FBR-81-1, Air Force Flight Dynamics Laboratory; 1971.
[45] Bathias C, Vancorn M. Mechanisms of overload effect on fatigue crack propagation in aluminum alloys. Eng Fract Mech 1978;10:409–24.
[46] Bretz PE, Vasudevan AK, Bucci RJ, Malcolm RC. Fatigue crack growth behaviour of 7XXX aluminum alloys under simple variable amplitude loading. In: Fracture mechanics, fifteenth symposium, ASTM STP 833. American Society for Testing and Materials; 1984. p. 242–65.